Eur. Phys. J. C (2014) 74:2736
DOI 10.1140/epjc/s10052-014-2736-3

THE EUROPEAN PHYSICAL JOURNAL C

Regular Article - Theoretical Physics

An analysis of elastic scattering reactions with a Fermi–Dirac pomeron opaqueness in impact parameter space

Claude Bourrely[a]

Département de Physique, Faculté des Sciences de Luminy, Aix-Marseille Université, 13288 Marseille Cedex 09, France

Received: 17 October 2013 / Accepted: 7 January 2014 / Published online: 6 February 2014

Abstract In the Bourrely–Soffer–Wu model we introduce for the pomeron a new opaqueness in impact parameter space in terms of different quark contributions described by a Fermi–Dirac distribution. In order to check the validity of this assumption we consider $p\ p$, $\bar{p}\ p$, and $\pi^{\pm}\ p$ elastic scattering. We emphasize the role of the gluon above the diffraction peak in the differential cross sections. Once these contributions are determined we extend the model to light nuclei elastic reactions like $p\ d$, $p\ ^4$He and $\pi^{\pm}\ ^4$He. The results obtained show a good description of all these elastic processes over the available experimental energy range and moderate momentum transfer.

1 Introduction

The advent of the LHC collider has renewed the interest of the high-energy behavior of the $p\ p$ elastic scattering and raises the question of the validity of numerous models devoted to this reaction. Many years ago we proposed the Bourrely–Soffer–Wu (BSW) model [1] and made further developments [2–4] to improve the agreement with experiments. This model which is based on an impact-picture phenomenology relies for the pomeron contribution to the opaqueness on two assumptions:

(i) the energy dependence is deduced from the high-energy behavior of quantum field theory [5,6];

(ii) the momentum transfer dependence follows from the supposed proportionality between the charge density of the proton and the internal distribution of matter [7–10].

With these simple assumptions we were able to obtain a good description of the available experimental data obtained at the ISR, SPS and Tevatron.

To be more precise, the assumption (ii) has led us to take for the momentum transfer dependence at the Born level a dipole in an analogous way to the approximation made to describe the proton electromagnetic form factor, however, this was not sufficient and an extra term was added (see next section). We stress that the relation between charge and matter density was never strictly proven, moreover, in this description we ignore the quark constituents of the proton, so the purpose of the paper is to find a new opaqueness expression which involves the proton constituents. The key observation is that in BSW the opaqueness in impact parameter b space is very similar to a Fermi function, so we propose that for each quarks we associate a Fermi component being dependent on the impact parameter b. Another justification of this new opaqueness is provided by our statistical model for parton distribution functions (PDF) and transverse parton distributions (TMD) which are built in with Fermi functions [11–13], the model is able to describe a large set of unpolarized and polarized structure functions in momentum space.

This idea to introduce a Fermi function in b space has been considered by several authors [14–16] and also in momentum space with a Tsallis function [17,18].[1] However, most authors consider a global opaqueness which does not discriminate between the quark components, and we will see that in our approach the properties of each of them reflect their importance inside the proton and that their associated thermodynamical potentials remain valid for light nuclei elastic reactions. Let us also mention the quark–diquark model [20,21] and the Generalized Parton Distributions (GPD), which are functions of b and the transverse momentum k_{T} [22].

The paper is organized as follows: after a brief introduction to the original BSW model in Sect. 2, we define in Sect. 3 a new expression for the opaqueness. In Sect. 4 we analyze the $p\ p$ and $\bar{p}\ p$ elastic scattering data which determine the free parameters, the relation between the matter distribution and the proton electromagnetic form factor is discussed in Sect. 5; then we extend our approach to $p\ d$ in Sect. 6 and

[a] e-mail: bourrely@cmi.univ-mrs.fr

[1] For a review see Ref. [19].

to p ^{4}He elastic scattering in Sect. 7. In order to check the validity of our assumption we consider also the π p and π ^{4}He elastic scattering in Sects. 8 and 9, respectively. The last section contains our conclusion.

2 A summary of the BSW model

In the BSW model [1–4] the amplitude is defined by the eikonal expression

$$a(s,t) = \frac{is}{2\pi}\int \mathrm{e}^{-i\mathbf{q}\cdot\mathbf{b}}(1-\mathrm{e}^{-\Omega(s,b)})\,\mathrm{d}\mathbf{b}, \tag{1}$$

where the opaqueness

$$\Omega(s,b) = S(s)F(b) + R(s,b), \tag{2}$$

the energy dependence is given by the complex crossing symmetric expression deduced from quantum field theory,

$$S(s) = \frac{s^c}{(\ln s)^{c'}} + \frac{u^c}{(\ln u)^{c'}}, \tag{3}$$

and in Eq. (2) $F(b)$ is the profile function related to the pomeron contribution and $R(s,\ b)$ represents Regge contributions which are added to describe the low-energy scattering. We define at the Born level the momentum transfer dependence through the product of a dipole multiplied by an extra function whose property is to avoid spurious dips at large momentum transfer in the differential cross sections. Therefore, the profile function reads

$$\tilde{F}(t) = f\,[G(t)]^2\,\frac{a^2+t}{a^2-t}, \tag{4}$$

$$G(t) = \frac{1}{(1-t/m_1^2)(1-t/m_2^2)}. \tag{5}$$

We will see that this extra function is in fact related to the gluon contribution. The scattering amplitude is expressed as a Bessel transform

$$a(s,t) = is\int_0^\infty J_0(b\sqrt{-t})(1-\mathrm{e}^{-\Omega(s,\mathbf{b})})b\,\mathrm{d}b, \tag{6}$$

we notice that the factorization property in Eq. (2) does not hold when the amplitude is eikonalized. In impact space the profile function reads

$$F(b) = \int_0^\infty \tilde{F}(t)J_0(b\sqrt{-t})\sqrt{-t}\,d\sqrt{-t}\,, \tag{7}$$

where the Bessel transform of $\tilde{F}(t)$ gives the dimensionless expression

$$\begin{aligned} F(b) = -f m_1^2 m_2^2 \Big\{ &\left[1+2a^2A_{13}\right]A_{12}^2 m_2^2 \frac{m_1 b}{2}K_1(m_1 b) \\ &+\left[1+2a^2A_{23}\right]A_{12}^2 m_1^2 \frac{m_2 b}{2}K_1(m_2 b) \\ &+\left[2+2a^2(A_{13}+A_{23})\right]A_{12}^3 m_1^2 m_2^2\,(K_0(m_1 b)-K_0(m_2 b)) \\ &+2a^2 m_1^2 m_2^2 A_{12}A_{32}A_{31} \\ &\times\left[A_{31}\,(K_0(m_1 b)-K_0(ab))-A_{32}\,(K_0(m_2 b)-K_0(ab))\right]\Big\}, \end{aligned} \tag{8}$$

the coefficients A_{ij} depend on $m_1,\ m_2,\ a$. In Eq. (8) the terms associated with the Bessel $K_0(ab)$ which depend on the parameter a introduced in (4) give a negative contribution to the sum. Conversely, we have

$$\tilde{F}(t) = \int_0^\infty F(b)J_0(b\sqrt{-t})b\,\mathrm{d}b. \tag{9}$$

A fit of the experimental data (see Ref. [3]) gives for the pomeron parameters the values we display in Table 1.

3 The Fermi–Dirac opaqueness

At the level of the BSW Born term in momentum space we used a modified dipole approximation, arguing that there should be some kind of similarity between the distribution of matter and the distribution of charge inside the proton. Taking the Fourier transform of this modified dipole we get the opaqueness $\Omega(s,b)$ in the impact parameter space b. Now, looking at the curve $F(b)$ in Fig. 2 of Ref. [1], we observe that its shape can be approximated by Fermi–Dirac functions.

We know from QCD that inside a proton its constituents are two quarks u, one d, a sea and the gluon; we can infer that each of them contributes to the profile function $F(b)$. From our previous observation we deduce that their global effect can be described by a Fermi function, so we make the hypothesis that the individual nature of these constituents is also of Fermi type and that the sum should reproduce the same profile function, $F(b)$, as in BSW.

Now, in analogy with the Fermi PDF expressions, which in $Q^2,\ x$ space depend on thermodynamical potentials and temperature, see Ref. [11–13], we propose to associate to each quark a Fermi function with a thermodynamical potential now in b space, namely, $X_u,\ X_d,\ X_{\bar{q}},\ X_g$, and a parameter b_0, which represents an average size localization of the partons inside the proton. For the gluon due to the boson nature we use a Bose–Einstein function and introduce a non-zero potential otherwise its contribution would be infinite for $b=0$. These properties can be summarized by the following crossing symmetric expression:

Table 1 Parameters of the BSW model

$c = 0.167$	$c' = 0.748$
$m_1 = 0.577$ GeV	$m_2 = 1.719$ GeV
$a = 1.858$ GeV	$f = 6.971$ GeV^{-2}

Table 2 Pomeron parameters of the Fermi model for $p\ p$ and $\bar{p}\ p$ elastic scattering

$c = 0.1677 \pm 0.0018$	$c' = 0.7103 \pm 0.0176$
$c_0 = 0.0891 \pm 0.0029$	$c_1 = 13.4678 \pm 0.238$
$c_2 = 21.6197 \pm 0.358$	$c_3 = 4.9707 \pm 0.242$
$b_0 = 0.3337 \pm 0.0098$ fm	$X_u = 0.269 \pm 0.0073$ fm
$X_d = 1.0654 \pm 0.011$ fm	$X_{\bar{q}} = 1.8837 \pm 0.03138$ fm
$X_g = 0.6832 \pm 0.014$ fm	

$$F(b) = c_0 \left[\frac{1}{1+\exp\left[\frac{b-X_d}{b_0}\right]} + \frac{c_1}{1+\exp\left[\frac{b-X_u}{b_0}\right]} + \frac{c_2}{1-\exp\left[\frac{b+X_g}{b_0}\right]} + \frac{c_3}{1+\exp\left[\frac{b+X_{\bar{q}}}{b_0}\right]} \right], \tag{10}$$

where the signs in front of the potentials are defined according to the same convention as in the case of parton distributions. Here, c_0 plays the role of the parameter f in BSW, the coefficients c_1, c_2 and c_3 are the relative weight of u, g and sea with respect to the quark d. We ignore in this first approach heavy quarks.

Our goal is to show that the expression (10) can be used to describe different elastic reactions and that, once the potentials are determined from $p\ p$ elastic scattering, their values are an *intrinsic property of the quarks*, also valid for scattering reactions involving light nuclei, and they give a reliable description of the proton electric form factor at low Q^2.

4 The $p\ p$ and $\bar{p}\ p$ elastic scattering

Now, it remains to determine the values of the above parameters by making a fit to the data. We use the same set of data as in the original BSW [31–45]; to be precise, the energy ranges from $p_{\rm lab} = 100$ GeV to $\sqrt{s} = 1.8$ TeV for $p\ p$ and $\bar{p}\ p$, and for the momentum transfer we restrict the values to $|t| < 5$ GeV^2. In order to put more constraints on the pomeron we take into account low-energy data, so we use for the Regge contributions the same expressions as in BSW [1,3]. A fit gives for the pomeron parameters the numerical values one finds in Table 2.

With these parameters we obtain a $\chi^2 = 2060$ for 955 pts which gives a $\chi^2/pt = 1.95$ and has to be compared with the BSW value $\chi^2/pt \sim 2.8$. We notice that the parameters

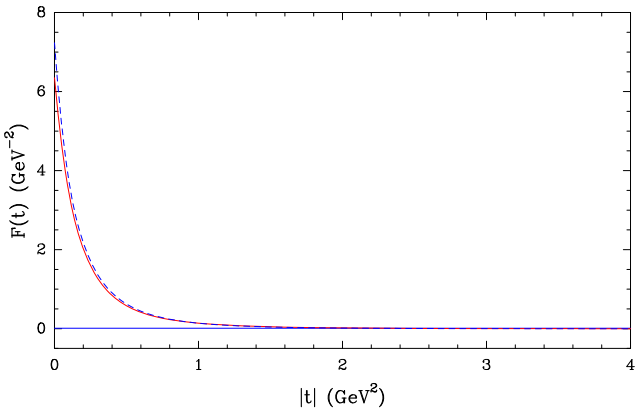

Fig. 1 The profile function $\tilde{F}(t)$ as a function of $|t|$ for pp scattering. Fermi *solid red curve*, BSW dashed *blue curve*

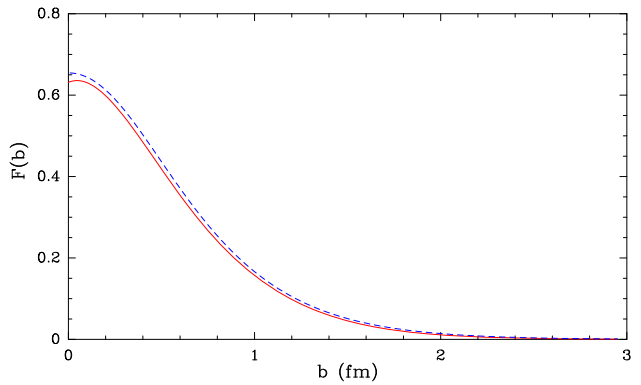

Fig. 2 The profile function $F(b)$ as a function of b for pp scattering. Fermi *solid red curve*, BSW *dashed blue curve*

c, c' are close to the ones obtained with BSW, which means that the asymptotic behavior of $S(s)$ is preserved.

We show in Fig. 1 the function $\tilde{F}(t)$ and in Fig. 2 the profile function $F(b)$ produced by the Fermi–Dirac functions; both of them are very close to the BSW curves. With the parameters of Table 2 the individual contribution of quarks to the profile function is shown in Fig. 3. We see that they are concentrated around 1 fermi, which is the expected size of the proton, the two quarks u in the proton give the main contribution compared to the d quark, the gluon has a contribution concentrated at small b.

We plot in Figs. 4 and 5 the differential cross sections for $p\ p$ and $\bar{p}\ p$, where we obtain good agreement with the data. The prediction at $\sqrt{s} = 7$ TeV shows that the Fermi version presents as BSW the same mismatch at large t compared with the TOTEM differential cross section measurement [23,24]; see Fig. 6. At this energy we predict $\sigma_{\rm tot} = 91.95 \pm 1.2$ mb, $\sigma_{\rm el} = 25.7 \pm 2.2$ mb, $\rho = 0.124$. These values have to be compared with the TOTEM data $\sigma_{\rm tot} = 98.0 \pm 2.5$ mb; notice that we agree with $\sigma_{\rm el} = 25.43 \pm 1.07$ mb and the position of the first minimum of the differential cross section. We show in Fig. 7 the behavior of the total and elastic cross sections.

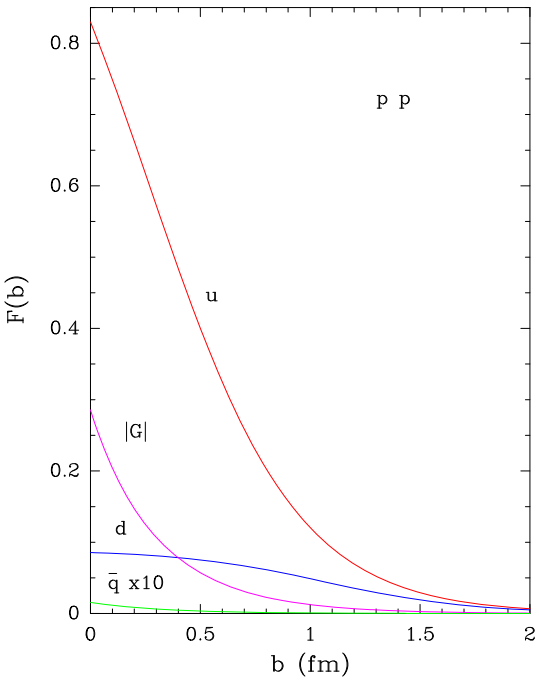

Fig. 3 Individual contribution of quarks to the profile function for pp scattering

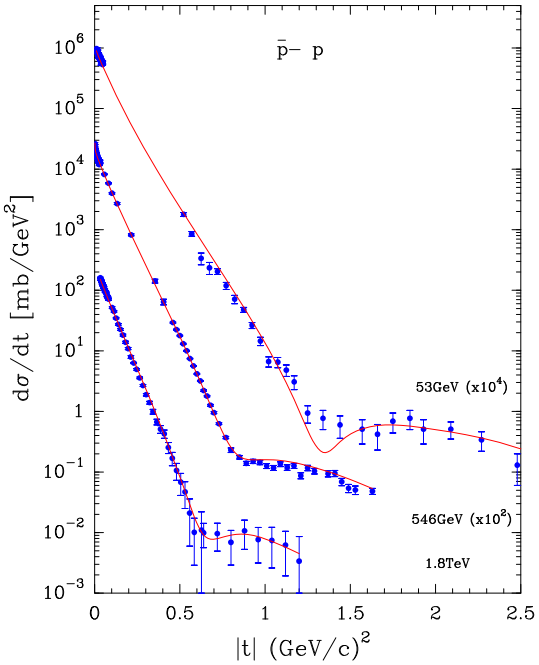

Fig. 5 The $\bar{p}p$ differential cross section as a function of $|t|$. Experiments from Refs. [34,35,37–45]

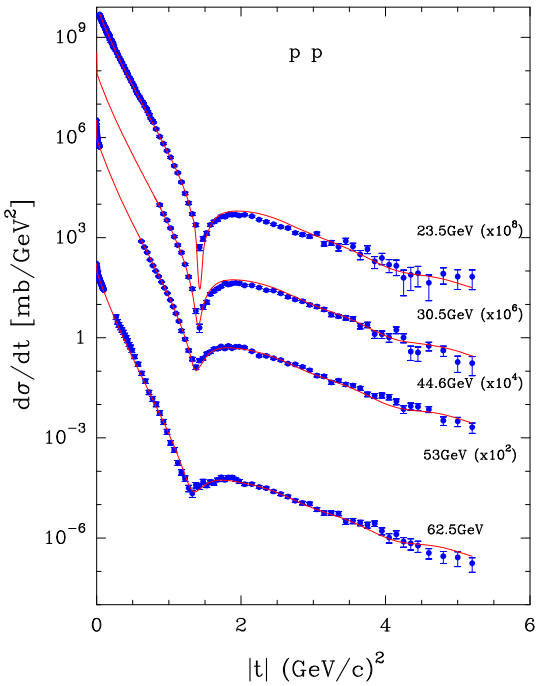

Fig. 4 The pp differential cross section as a function of $|t|$. Experiments from Refs. [31–36]

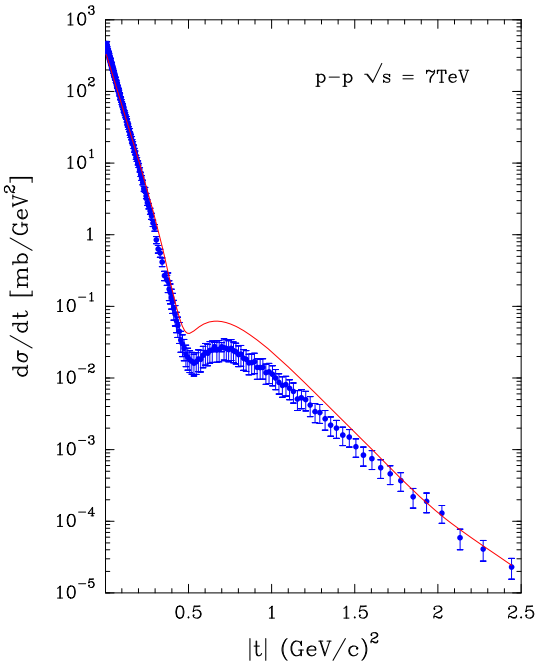

Fig. 6 A prediction of the Fermi model compared to the TOTEM experimental data [23,24]

Let us make a comment: the inclusion the TOTEM data in our fit notably increases the χ^2, so the quoted parameters values are obtained leaving aside these data. A discussion of the BSW model with respect to the TOTEM data is reported in Ref. [25]. In fact, our pomeron, whose energy dependence is controlled by the parameters c, c', which are constrained by a fit in an energy range from low energy up to 1.8 TeV cannot give a total cross section as high as the one obtain by TOTEM. In order to reach this value we need a revision of the pomeron behavior, but before making any modification we wait for a

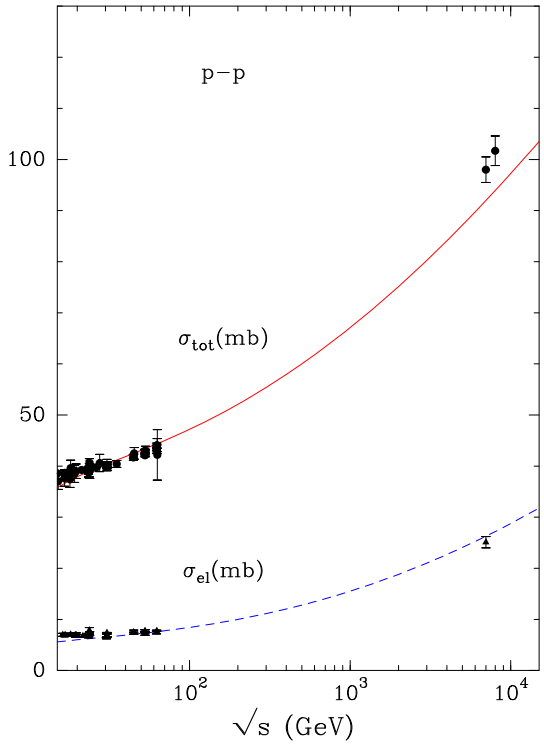

Fig. 7 The pp total and elastic cross sections as a function of $\sqrt{s}$. Experimental data from Refs. [23,46]

confirmation from another experiment [26,27]. Let us point out that at the Tevatron energy 1.8 TeV we obtain $\sigma_{tot} = 73.6 \pm 1.5$ mb which is in agreement within the experimental range $71.42 \leq \sigma_{\rm tot} \leq 80.03$ mb with an average error 2.4 mb [28–30]. Notice that the values of the above parameters c, c' are perfectly compatible with the high-energy behavior of light nuclei reactions discussed in the next sections.

The role of the gluon

In the Born term Eq. (4) of BSW we have introduced the extra term $\frac{a^2+t}{a^2-t}$ in order to cancel a spurious second dip in the differential cross section; this term implies that $\tilde{F}(t)$ has a zero at $|t| = a^2 = 3.74\,\text{GeV}^2$ and becomes negative above. The Bessel transform of the Fermi distribution (10) with respect to b gives a function $\tilde{F}(t)$ which has also a zero at $|t| = 4.3\,\text{GeV}^2$ and a negative value above, see Fig. 1. We will show that the origin of this zero is produced in fact by the gluon as we now explain.

Looking at the expression of $F(b)$ Eq. (10) we see that it contains four terms, including the u, d, the sea, and the gluon contributions. Let us suppose that we remove the gluon contribution, a fit made with only the u and d and the sea gives a very large χ^2, moreover, $\tilde{F}(t)$ has no zero, so one can conclude that the gluon contribution is necessary to obtain a reasonable χ^2 and to produce a zero in $\tilde{F}(t)$. Concerning the gluon, a more detailed comparison between the Fermi and the BSW approaches can be made. When making a plot of Eq. (8) we observe that the terms associated with Bessel functions whose arguments depend on m_1 or m_2 give a positive contribution to $F(b)$, while terms associated with the parameter a give a negative contribution. In the Fermi case the gluon has a denominator $1-\exp\left[\frac{b+X_g}{b_0}\right]$ where the minus sign reflects the Bose nature of the contribution. Now the value of the potential X_g must be such that the denominator never vanishes; otherwise we get a singularity, and taking also into account the constraint for $b = 0$ we see that the denominator must be always negative. This makes obvious a clear correspondence between the gluon and the contribution due to the term associated with the parameter a in BSW.

5 The proton electric form factor at low Q^2

In Sect. 2, we have introduced the BSW profile function $\tilde{F}(t)$ Eq. (4), which depends on $G^2(t)$ (Eq. 5), interpreted as a nuclear form factor. In Sect. 3, we have defined a new $\tilde{F}(t)$ as the Bessel transform of the Fermi–Dirac expressions (10). Now, we raise the question if there is any relation between this nuclear form factor and the electromagnetic form factor of the proton. To this end, we define using Eq. (10) the proton electric form factor by the expression

$$G_e^2(Q^2) = \int_0^\infty b\,\mathrm{d}b J_0(bQ) f_e^2 \left[\frac{1}{1+\exp\left[\frac{b-X_d}{b_e}\right]} + \frac{c_1}{1+\exp\left[\frac{b-X_u}{b_e}\right]} + \frac{c_2}{1-\exp\left[\frac{b+X_g}{b_e}\right]} + \frac{c_3}{1+\exp\left[\frac{b+X_{\bar{q}}}{b_e}\right]} \right]. \quad (11)$$

Compared to Eq. (10) we introduce the normalization factor f_e^2 and replace the quarks extension b_0 inside the proton by b_e, which corresponds to the electromagnetic case, and all the other parameters are kept fixed at the values given in Table 2. The normalization factor f_e^2 is determined by the condition $G_e(0) = 1$, and we obtain $f_e^2 = 0.0143\ \text{GeV}^2$ and the best agreement with the experimental form factor data gives $b_e = 0.326$ fm—a value slightly less than $b_0 = 0.337$ fm. We can interpret this small difference by the fact that u quarks give the most important contribution at small b (see Fig. 3) and carry 4/3 of the charge, while the d quark, giving a smaller contribution, has a charge $-1/3$.

In order to make a comparison with experiment we have to rely on the available measured ratio $G_e(Q^2)/G_{\rm dipole}(Q^2)$[2] since we are not able to compute the magnetic form factor, so we cannot use the measurements of G_e/G_m. In Fig. 8 we show the plot $G_e(Q^2)/G_{\rm dipole}(Q^2)$ produced by the Fermi

[2] $G_{\rm dipole}(Q^2) = \frac{1}{(1+Q^2/0.71)^2}$ is the usual dipole form factor.

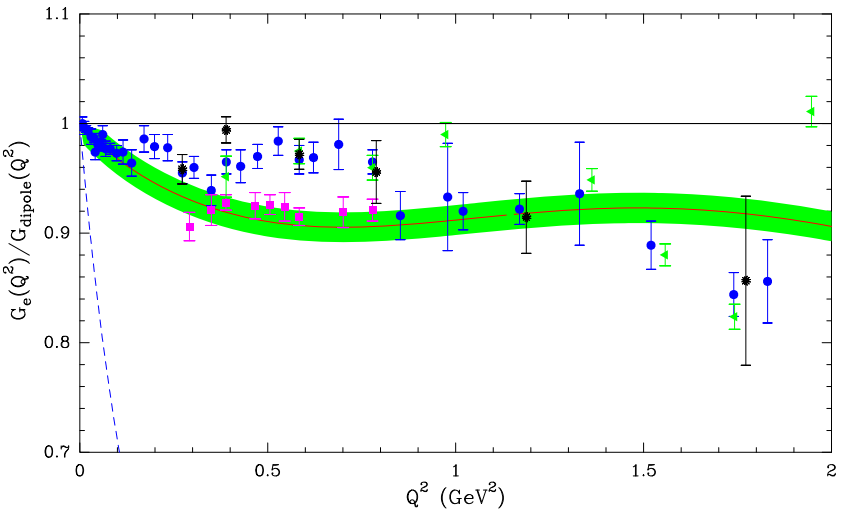

Fig. 8 The proton electric form factor $G_e(Q^2)$ normalized to G_{dipole} as a function of Q^2. Fermi *solid curve*, uncertainty domain *shaded area*, BSW *dashed curve*. Experimental data: *square* [47,48], *triangle* [49], *star* [50], *circle* a data analysis presented in Ref. [51]

distributions (11) (solid line), the agreement with experimental data at low Q is relatively good, we notice that the recent polarized experiment at JLab [47,48] (squares in the figure) gives the most precise values. For reference we show the case of BSW given by Eq. (4); we observe a fast decrease of this ratio, because the parameters m_1 and m_2 are only valid in the nuclear case.

In the introduction we raised the question of a possible relation between the nuclear and electromagnetic form factors; our Fermi approach shows clearly that with only two new parameters we can make a close link between the distribution of matter and the distribution of charge inside the proton.

6 The *p d* elastic scattering

In the previous section we considered elastic scattering between two elementary particles $p\ p$, $\bar{p}p$ and found the basic properties of quarks, sea, and gluon interaction through a Fermi–Dirac function in impact parameter space. The question arises how to extend this type of interaction when a light nucleus like the deuteron is involved in the $p\ d$ elastic scattering.

Our theoretical input for the profile function is the same formula defined for $p\ p$ by Eq. (10), where we keep the same value of the parameters c, c' and the thermodynamical potentials; the only free parameters are the normalization coefficients c_0, c_1, c_2, c_3, and the parameter b_0 associated with the deuteron size. We infer that the total cross section for this process is higher than in the proton case; c_0 must increase.

The experimental data [53–55] cover the energy range $40 \leq p_{\text{lab}} \leq 397$ GeV and the momentum transfer range $0.00077 \leq |t| \leq 0.2435$ GeV^2 [53–55]. Of course, the energy domain is more limited than in the $p\ p$ reaction, and

Table 3 Pomeron parameters of the Fermi model for $p\ d$ elastic scattering

$c_0 = 0.0726 \pm 0.002$	$c_1 = 33.1219 \pm 0.229$
$c_2 = 7.4228 \pm 0.0.23$	$c_3 = -35.592 \pm 1.09$
$b_0 = 0.544 \pm 0.0122$ fm	

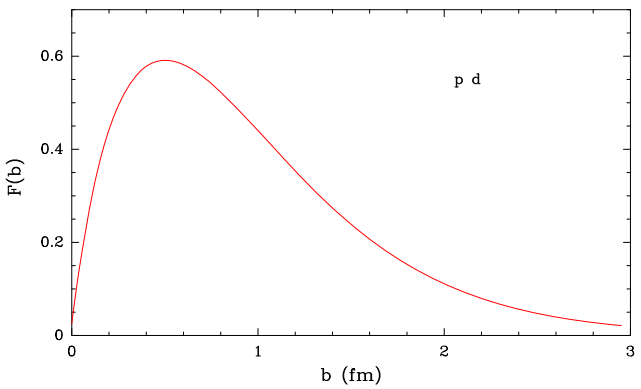

Fig. 9 The profile function $F(b)$ as a function of b

the momentum transfer covers only low $|t|$ values; nevertheless, we find it interesting to check the validity of our assumption on the universality of the thermodynamical potentials in this case. After a fit of the data we obtain $\chi^2 = 1533$ for 1000 pts, giving a $\chi^2/pt = 1.53$, which is slightly better than the proton value. The resulting parameters for the pomeron are given in Table 3.

The profile function $F(b)$ shown in Fig. 9 differs from the $p\ p$ case with a maximum at $b = 0.5$ fm. In Fig. 10 we plot the different components of the pomeron contribution, we observe that the gluon and the quark u give the major contribution. The differential cross sections show a perfect agreement with the data in the measured low t region; see Figs. 11 and 12. Concerning the total cross we obtain for

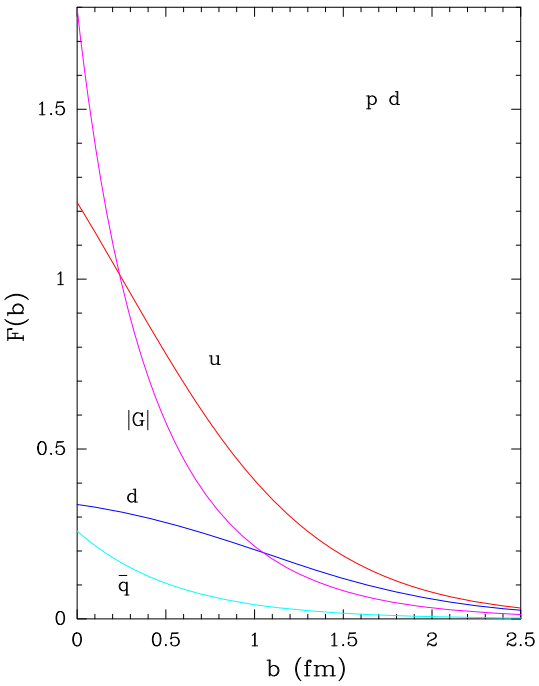

Fig. 10 Individual contribution of quarks to the profile function for $p-d$

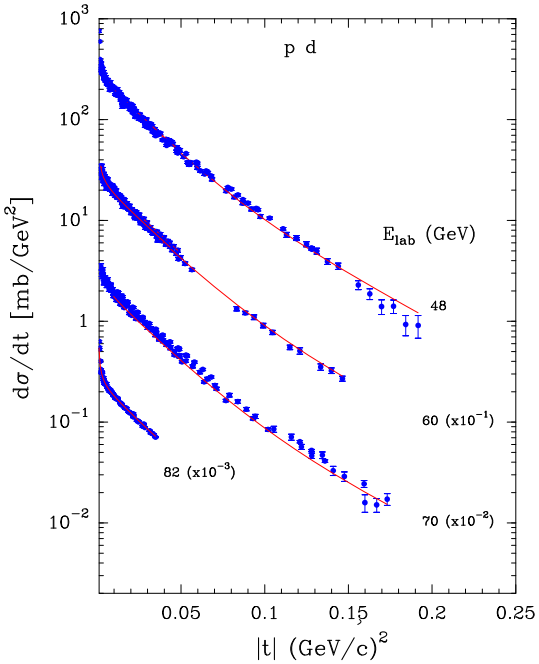

Fig. 11 The pd differential cross section as a function of $|t|$. Experiments from Refs. [53–55]

instance at $E_{\rm lab} = 240$ GeV, $\sigma_{\rm tot} = 73.77 \pm 0.4$ mb, to be compared with the experimental value 74.42 ± 0.53 mb [52]

This result confirms that our basic Fermi interaction between quarks obtained in the elastic proton case, where we have a system made of $4u + 2d$, remains valid for this light nucleus scattering where now it contains $5u + 4d$.

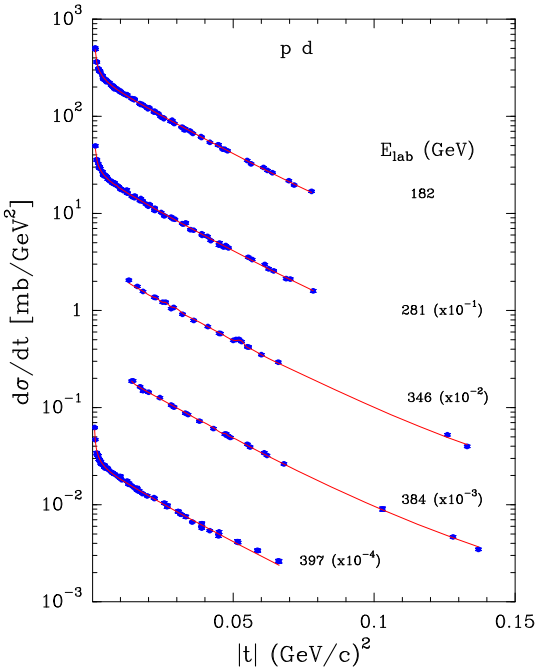

Fig. 12 The pd differential cross section as a function of $|t|$ continued

Table 4 Pomeron parameters of the Fermi model for p ^{4}He elastic scattering

$c_0 = 0.0134 \pm 0.0015$	$c_1 = 29.9041 \pm 1.01$
$c_2 = 24.9568 \pm 1.02$	$c_3 = 0.4968 \pm 0.067$
$b_0 = 0.5967 \pm 0.0018$ fm	

7 The p ^{4}He elastic scattering

Following the same approach as the previous sections, we propose to describe the elastic reaction p ^{4}He from the measurements made at Fermilab with a gas target in a range of energies from 97 to 400 GeV and momentum transfer $0.003 \leq |t| \leq 0.52$ GeV^2 [56,57].

Our theoretical input for the profile function relies on the same formula defined for $p\ p$ by Eq. (10) where we keep the same value of the parameters c, c' and the thermodynamical potentials; here again the only free parameters are the coefficients c_0, c_1, c_2, c_3, and the parameter b_0.

A fit gives a $\chi^2 = 476$ for 504 pts or a $\chi^2/pt = 0.94$. The resulting parameters for the pomeron are given in Table 4:

With these parameters we plot in Fig. 13 the different components of the pomeron contribution, we observe that the gluon and the quark u give the major contribution a situation similar to the $p\ d$ case (see Fig. 10). A plot of the differential cross sections is shown in Fig. 14; we notice that the dip region is well described. Concerning the total cross we obtain at $E_{\rm lab} = 250$ GeV $\sigma_{\rm tot} = 132.13 \pm 0.5$ mb, to be compared

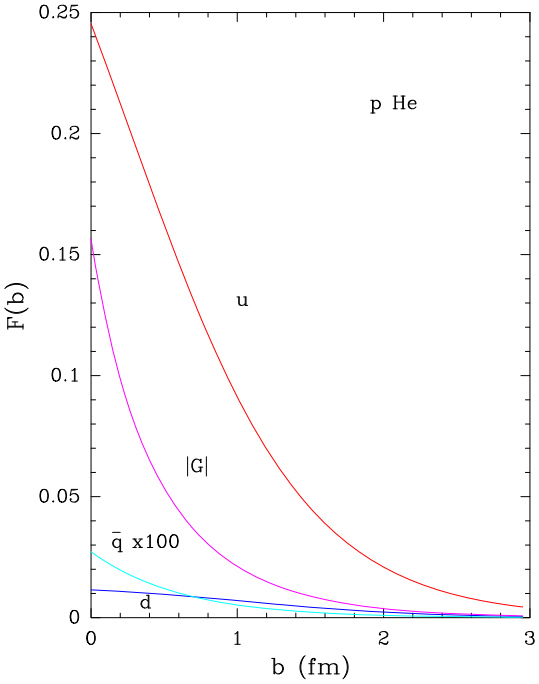

Fig. 13 Individual contribution of quarks to the profile function for p ^{4}He

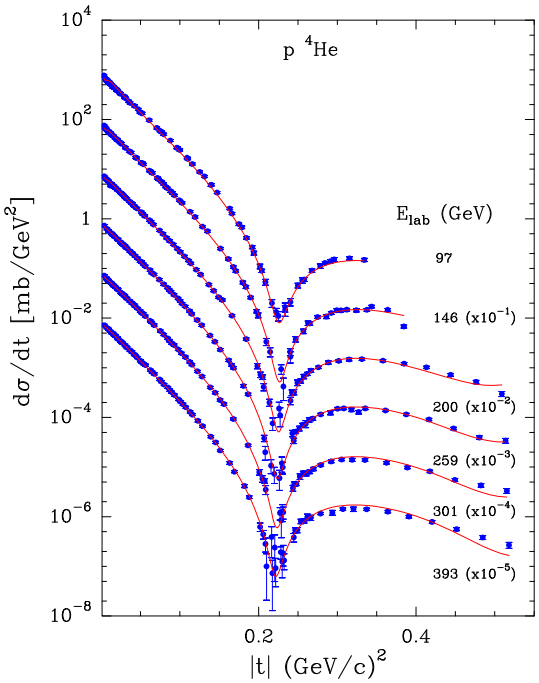

Fig. 14 The p ^{4}He differential cross section as a function of $|t|$. Experiments from Refs. [56,57]

with $\sigma_{\rm tot} = 131.6 \pm 0.8$ mb of Ref. [57]. For this reaction the agreement with the data validates our assumption on the structure of the profile function $F(b)$ and the fact that the thermodynamical potentials are kept the same.

8 The $\pi^{\pm}$ p elastic scattering

In addition to p p scattering the $\pi^{\pm}$ p must give new information on the partons content of the π p interaction. For this reaction, in the original BSW the pomeron contribution is defined by the expression

$$\tilde{F}(t) = f_\pi G(t) \mathcal{F}_\pi(t) \frac{a_\pi^2 + t}{a_\pi^2 - t}, \tag{12}$$

where $\mathcal{F}_\pi(t) = \frac{1}{1 - t/m_{3\pi}^2}$ is a simple pole, and from a fit we obtained the following parameters:

$$m_{3\pi} = 0.7665 \text{ GeV}, \quad f_\pi = 4.2414, \quad a_\pi = 2.3272 \text{ GeV}. \tag{13}$$

For the Fermi description of the π p interacting system in impact parameter space we explore a slightly different approach compared to the proton case, in the sense that we introduce a different quark potential according to the charge of the pion so that the new pomeron profile function takes the form

$$F_\pi^{\pm}(b) = d_0 \left[\frac{1}{1 + \exp[\frac{b - X_d^{\pm}}{b_0}]} + \frac{d_1}{1 + \exp[\frac{b - X_u^{\pm}}{b_0}]} + \frac{d_2}{1 - \exp[\frac{b + Z_g}{b_0}]} + \frac{d_3}{1 + \exp[\frac{b + Z_{\bar{q}}}{b_0}]} \right]. \tag{14}$$

Since the quark structure for π^+ is $u\,\bar{d}$ and for π^- is $d\,\bar{u}$, we define a set of thermodynamical potentials $X_u^{\pm}$, $X_d^{\pm}$ corresponding to $\pi^{\pm}$, the reason being that in the system at rest we have $3u + d$ for π^+ and $2u + 2d$ for π^-. Therefore, the potentials are not necessarily the same as in pp. For the sea we introduce a global potential $Z_{\bar{q}}$, and for the gluon component a potential Z_g. The parameters c, c', which drive the asymptotic energy behavior, are kept the same as in p p (see Table 2).

A simultaneous fit of $\pi^{\pm}$ data for $p_{\rm lab}$ = 100–250 GeV and momentum transfer $|t| < 2.5$ GeV^2 [58–62] gives a $\chi^2 = 1005$ with 608 pts or a $\chi^2/pt = 1.65$. The resulting parameters for the pomeron are given in Table 5.

Table 5 Pomeron parameters of the Fermi model for $\pi^{\pm}$ p elastic scattering

$d_0 = 3.4408 \pm 0.118$	$d_1 = 2.406 \pm 0.21$
$d_2 = 2.5345 \pm 0.195$	$d_3 = 5.5128 \pm 0.323$
$X_u^+ = 0.2802 \pm 0.002$ fm	$X_u^- = 0.2307 \pm 0.0197$ fm
$X_d^+ = 0.0096 \pm 0.0004$ fm	$X_d^- = 0.1772 \pm 0.0065$ fm
$Z_{\bar{q}} = 0.6323 \pm 0.0118$ fm	$Z_g = 0.3537 \pm 0.0116$ fm
$b_0 = 0.3096 \pm 0.004$ fm	

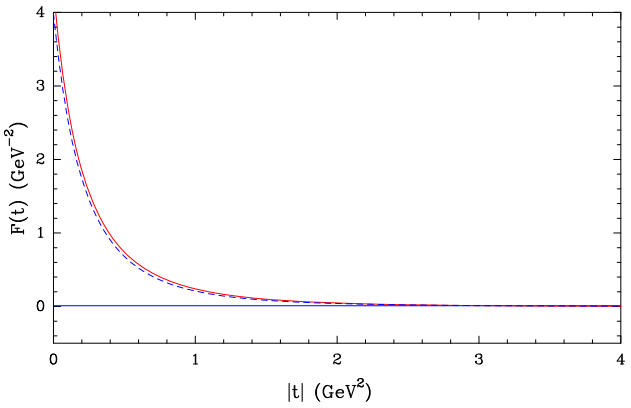

Fig. 15 The profile function $\tilde{F}(t)$ as a function of $|t|$ for $\pi^{\pm}$ p. Fermi *solid red curve*, BSW *dashed blue curve*

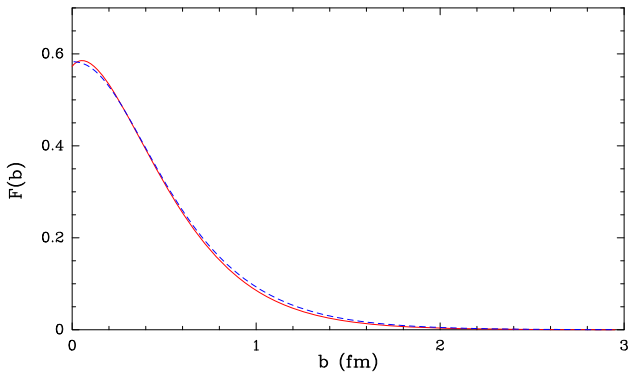

Fig. 16 The profile function $F(b)$ as a function of b for $\pi^{\pm}$ p. Fermi *solid red curve*, BSW *dashed blue curve*

Notice that the parameters $d_0, d_1, d_2, d_3, b_0, Z_{\bar{q}}, Z_g$ are the same for both reactions. In Figs. 15 and 16 a plot is made for $\tilde{F}(t)$ and $F(b)$ with a comparison to the BSW profile, the curves are very close, which shows the validity of the Fermi profile. The variation of $\tilde{F}(t)$ in π p for BSW shows a zero at $|t| = 5.6$ GeV^2, while for Fermi the zero occurs at $|t| = 6.9$ GeV^2, and this difference in the zero position reflects the dominance of the gluon over the sea as seen in Fig. 17.

Compared to p p scattering we do not have the same range of high-energy data so the pomeron parameters are subject to less constraints, nevertheless it is interesting to determine the size of the different components in Eq. (14). With the parameters of Table 5 we plot in Fig. 17 the individual contribution of the components in the π^+ p case. We observe the dominance of the quark u and the gluon, but the sea contribution, which was small in p p (see Fig. 3), becomes more sizeable, which is expected due to the pion effect.

We have introduced In Eq. (14) the potentials $X_u^{\pm}$, $X_d^{\pm}$ in order to separate the reactions $\pi^{\pm}$ leading to two separated profiles $F_{\pi}^{\pm}(b)$; with the parameters of Table 5 the numerical

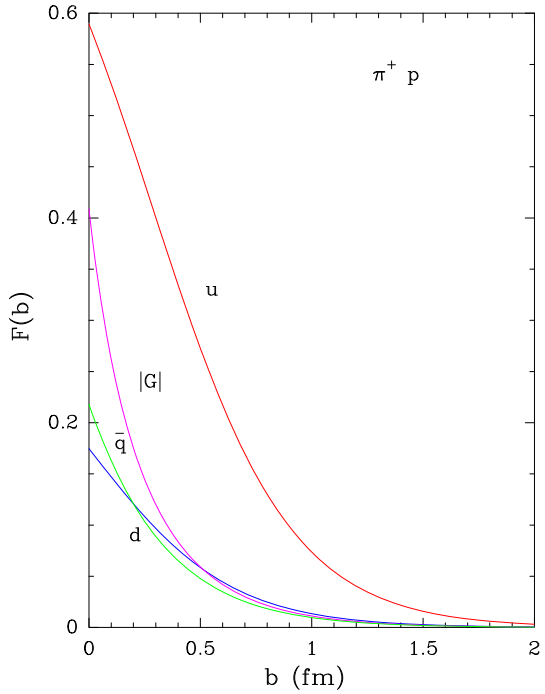

Fig. 17 Individual contribution of quarks to the profile function for $\pi^{\pm}$ p

difference between $F_{\pi}^{+}(b)$ and $F_{\pi}^{-}(b)$ is very small, and this fact can be explained by the experimental the differential cross sections for the two processes which are close in the energy range considered here, we remark that the difference is in part due to the Regge ρ contribution.

In Figs. 18 and 19 a plot of the differential cross sections shows a reasonable agreement with the data. Also, the large $|t|$ values presented in Fig. 20 reveal the existence of a dip around $|t| = 4.5$ GeV^2 consistent with the data. For the total cross sections we obtain at $p_{\text{lab}} = 310$ GeV a value $\sigma_{\text{tot}} = 24.86 \pm 0.2$ mb for π^- p and $\sigma_{\text{tot}} = 24.48 \pm 0.3$ mb for π^+ p, the experimental values are, respectively, $\sigma_{\text{tot}} = 24.9 \pm 0.08$ mb and $\sigma_{\text{tot}} = 24.5 \pm 0.1$ mb from Ref. [52]. Since we have a different pomeron potential for π^- and π^+, as regards the incidence on the total cross section at high energy, a prediction at $\sqrt{s} = 7$ TeV gives, respectively, for the two reactions 58.8 and 58.2 mb, the difference is 1 %, so the near equality of the cross sections at high energy is preserved in accordance with the Pomeranchuk theorem.

9 The $\pi^{\pm}$ ^{4}He elastic scattering

To study this reaction we follow the same approach as in the previous sections, namely, we keep the parameters c, c', and the thermodynamical potentials identical to those of the π p case. The parameters are determined from a fit of the CERN

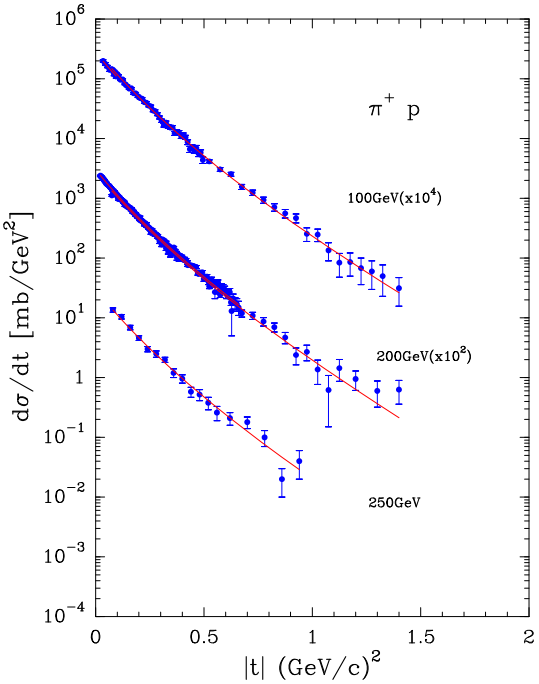

Fig. 18 The $\pi^+ p$ differential cross section as a function of $|t|$. Experiments from Refs. [58–62]

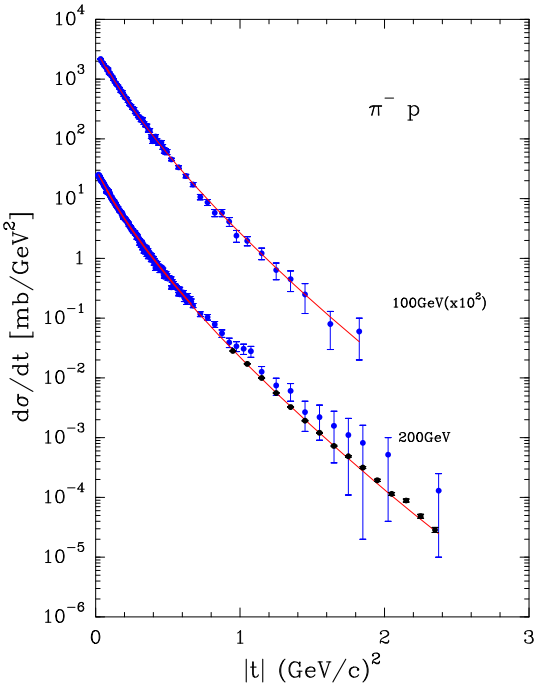

Fig. 19 The $\pi^- p$ differential cross section as a function of $|t|$. Experiments from Refs. [58–61]

data [57] for $50 \leq E_{\text{lab}} \leq 300$ GeV and a $|t|$ domain between 0.0086–0.0481 GeV^2. We obtain a $\chi^2 = 640$ for 584 pts or a $\chi^2/pt = 1.1$, which is close to the pion–proton value. The obtained parameters for the pomeron are given in Table 6:

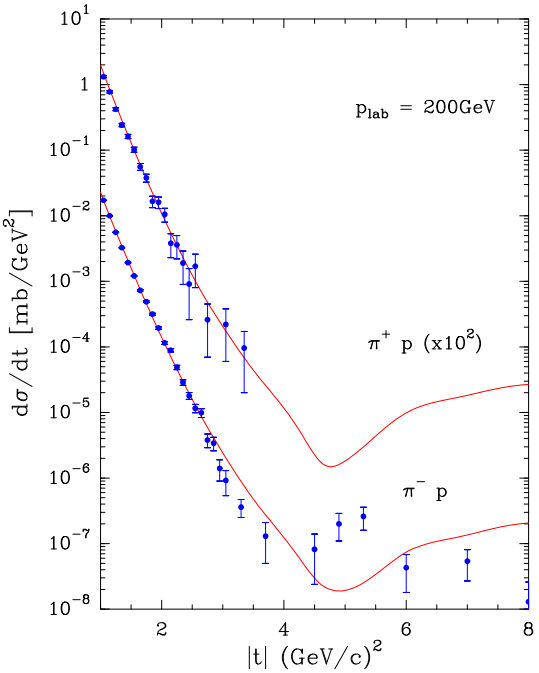

Fig. 20 The $\pi^{\pm} p$ differential cross section for large $|t|$ values. Experiment from Ref. [59]

Table 6 Pomeron parameters of the Fermi model for $\pi^{\pm}$ ^{4}He elastic scattering

$d_0 = 0.072 \pm 0.007$	$d_1 = 17.98699 \pm 1.03$
$d_2 = 23.262 \pm 1.20$	$d_3 = 46.306 \pm 2.215$
$b_0 = 0.5640 \pm 0.0124$ fm	

The parameter b_0 has the same order of magnitude as the one obtained in p ^{4}He. The different quark components are plotted in Fig. 21; we see that the gluon, the quark u, and the sea give the major contributions.

We show in Figs. 22 and 23 a plot of differential cross sections, although the t range is limited to the forward direction, the agreement with the data remains good. In Fig. 24 we make a prediction for the large $|t|$ π^- ^{4}He differential cross section at the highest measured energy, 300 GeV; a dip occurs at $|t| = 0.3$ GeV^2, which is slightly shifted to higher $|t|$ value compared to the reaction p ^{4}He (see Fig. 14).

For the total cross sections we obtain at $E_{\text{lab}} = 150$ GeV a value $\sigma_{\text{tot}} = 83.6 \pm 0.2$ mb for π^- ^{4}He and $\sigma_{\text{tot}} = 85.17 \pm 0.3$ mb for π^+ ^{4}He, the experimental values are, respectively, $\sigma_{\text{tot}} = 83.0 \pm 0.9$ mb and $\sigma_{\text{tot}} = 85.3 \pm 0.7$ mb from Ref. [57].

In the previous sections we made an analysis of eight reactions, $p\ p$, $\bar{p}\ p$, $p\ d$, p ^{4}He, $\pi^{\pm}\ p$, $\pi^{\pm}$ ^{4}He. The parameter b_0 introduced in the profile function of Eqs. (10) and (14) is related to the average size of the interacting parton system. We show in Fig. 25 a plot of the b_0 values as a function of the number of quarks u and d which are involved in a

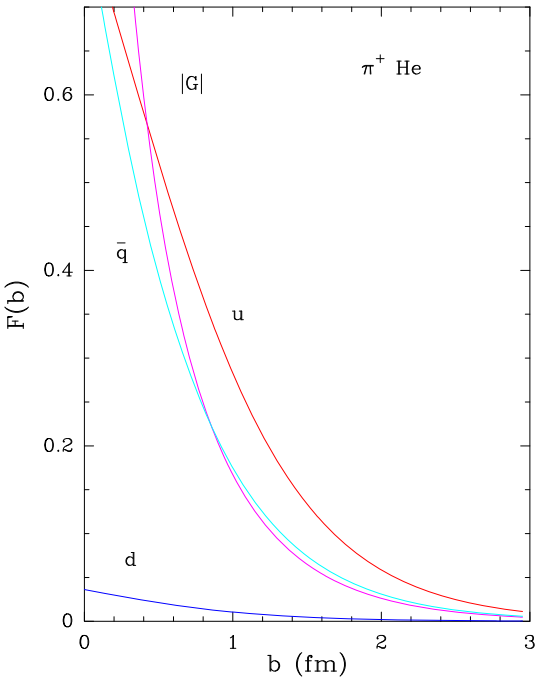

Fig. 21 Individual contribution of quarks to the profile function as a function of b for π^+ ^{4}He

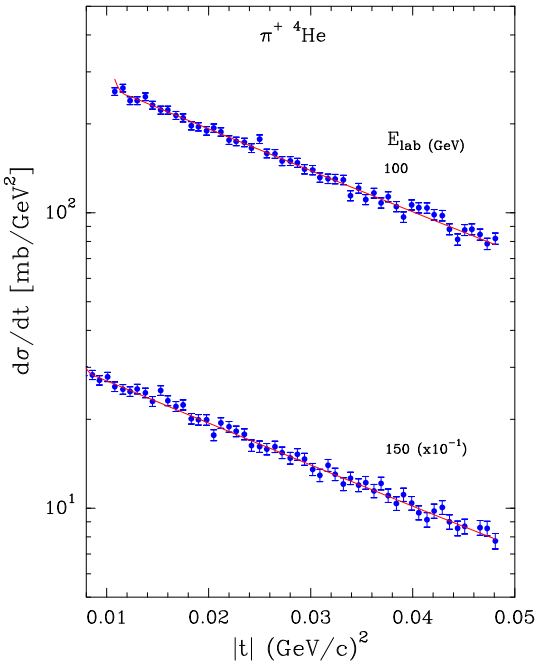

Fig. 23 The π^+ ^{4}He differential cross section as function of $|t|$. Experiment from Ref. [57]

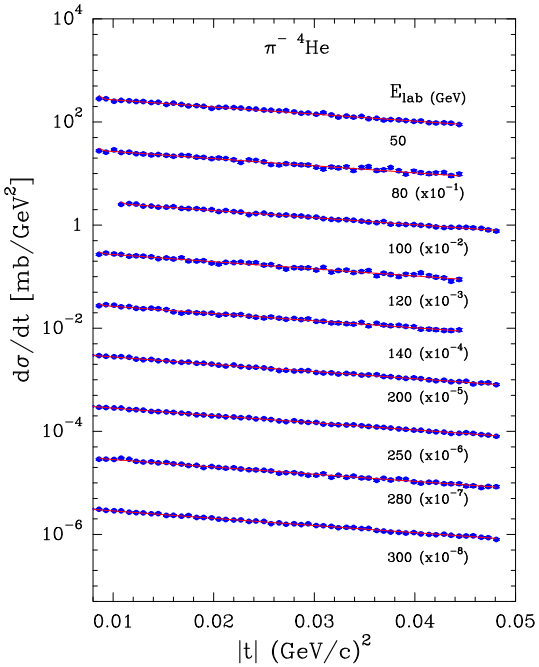

Fig. 22 The π^- ^{4}He differential cross section as function of $|t|$. Experiment from Ref. [57]

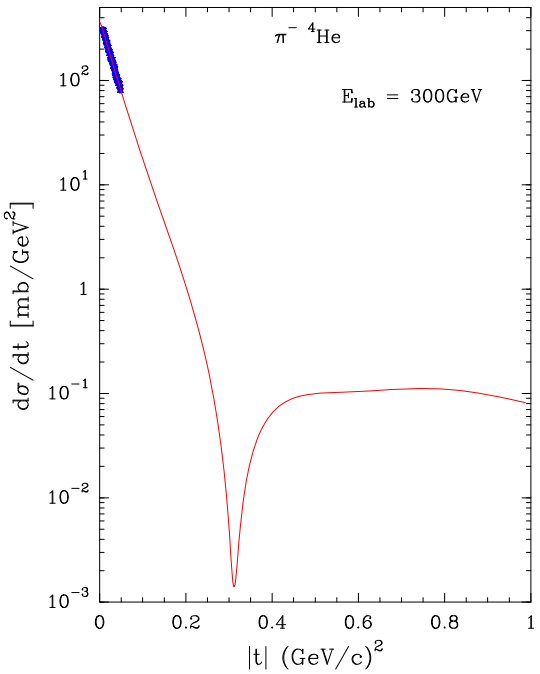

Fig. 24 π^- ^{4}He differential cross section at large $|t|$ values. Experiment from Ref. [57]

reaction, and we observe an increase of the b_0 values *with*, the number of quarks—an expected feature but interesting to confirm. This result is similar to the well-known nuclear situation where the mean radius of a nucleus increases with the corresponding atomic mass number.

10 Conclusion

The introduction of Fermi–Dirac functions as a new opaqueness built in with different parton components in impact parameter space gives a reasonable description of the eight

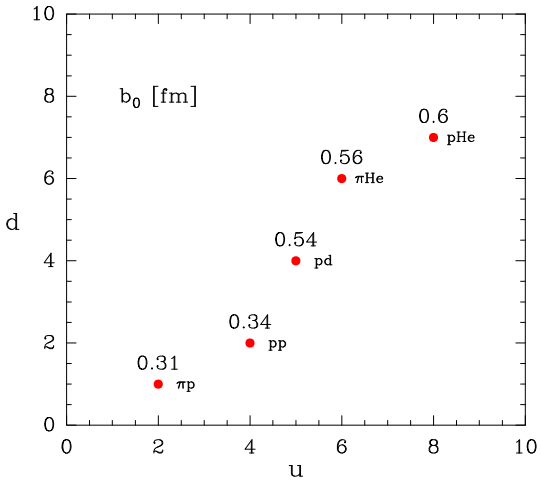

Fig. 25 The b_0 values as functions of u and d quarks number

elastic reactions $p\ p$, $\bar{p}\ p$, $p\ d$, p ^{4}He, $\pi^{\pm}\ p$, and $\pi^{\pm}\ ^4$He. The size and the behavior of these components in impact parameter space agrees with what we expect in their localization inside the interaction domain. This first simplified approach certainly needs a more refined version introducing heavy quarks and also reducing the number of parameters.

We would like to emphasize that we do not have to rely on the assumption of proportionality between the matter distribution and the charge distribution, which was introduced arbitrarily in the original BSW because in our Fermi approach the relation is obtained in a natural way. In BSW the presence of the extra term in $\tilde{F}(t)$ to cancel a second dip, which was never justified, is now explained by the role of the gluon. We have also proven that the thermodynamical potentials associated with the partons and determined from the basic interactions in $p\ p$ and $\pi\ p$ elastic scattering are an intrinsic property of the partons and also valid for elastic light nuclei reactions.

With the same approach one could envisage an extension to the spin amplitudes, where for each parton one defines two potentials related to the spin orientation up–down, in an analogous way to the polarized PDF [11–13]. However, due to the scarce measurements of polarized elastic reactions at high energy there exists the difficulty to obtain reliable values of the parameters.

Acknowledgments I am grateful to J. Soffer for constructive comments in the preparation of the manuscript.

References

1. C. Bourrely, J. Soffer, T.T. Wu, Phys. Rev. D **19**, 3249 (1979)
2. C. Bourrely, J. Soffer, T.T. Wu, Nucl. Phys. B **247**, 15 (1984)
3. C. Bourrely, J. Soffer, T.T. Wu, Eur. Phys. J. C **28**, 97 (2003)
4. C. Bourrely, J. Soffer, T.T. Wu, Eur. Phys. J. C **71**, 1061 (2011)
5. H. Cheng, T.T. Wu, Phys. Rev. Lett. **24**, 1456 (1970)
6. H. Cheng, T.T. Wu, *Expanding Protons: Scattering at High Energies* (M.I.T. Press, Cambridge, 1987)
7. T.T. Wu, C.N. Yang, Phys. Rev. **137**, B708 (1965)
8. T. Chou, C.N. Yang, Phys. Rev. **170**, 1591 (1968)
9. T. Chou, C.N. Yang, Phys. Rev. **175**, 1832 (1968)
10. T. Chou, C.N. Yang, Phys. Rev. Lett. **20**, 1213 (1968)
11. C. Bourrely, F. Buccella, J. Soffer, Eur. Phys. J. C **23**, 487 (2002)
12. C. Bourrely, F. Buccella, J. Soffer, Mod. Phys. Lett. A **18**, 771 (2003)
13. C. Bourrely, F. Buccella, J. Soffer, Eur. Phys. J. C **41**, 327 (2005)
14. M.M. Islam, R.J. Luddy, A.V. Produkin, Int. J. Mod. Phys. A **21**, 1 (2006). [arXiv:0508.200 [hep-ph]]
15. P. Brogueira, J. Dias de Deus, Eur. Phys. J. C **37**, 075006 (2010). [arXiv:1005.3644 [hep-ph]]
16. V. Uzhinsky, A. Galoyan [arXiv:1210.7338 [hep-ph]]
17. J. Cleymans, 1st International Conference on New Frontiers in Physics ICFP (2012) [arXiv:1210.7464 [hep-ph]]
18. J. Cleymans, G.I. Lykasov, A.S. Parvan, A.S. Sorin, O.V. Teryaev, D. Worku [arXiv:1302.1970 [hep-ph]]
19. I.M. Dremin, Phys. Uspekhi **56**, 3 (2013). [arXiv:1206.5474 [hep-ph]]
20. A. Bilias, A. Bzdak, Acta Phys. Pol. B **38**, 159 (2007). [arXiv:0612.038 [hep-ph]]
21. F. Nemes, T. Csörgő, J. Mod. Phys. A **27**, 1250175 (2012). [arXiv:1204.5617 [hep-ph]]
22. A.V. Belitsky, A.V. Radyushkin, Phys. Rep. **418**, 1 (2005). [arXiv:0504.030 [hep-ph]]
23. G. Antchev et al., TOTEM Collaboration, Europhys. Lett. **95**, 41001 (2011)
24. G. Antchev et al., Europhys. Lett. **96**, 21002 (2011) (CERN-PH-EP-2012-239)
25. A.K. Kohara, E. Ferreira, T. Kodama [arXiv:1212.3652 [hep-ph]]
26. ATLAS/ALFA Collaboration, CERN/LHCC/2008-004 2008
27. P. Puzo, AIP Conf. Proc. **1105**, 105 (2009)
28. N.A. Amos et al., Phys. Rev Lett. **68**, 2433 (1992)
29. F. Abe et al., Phys. Rev. D **50**, 5550 (1994)
30. C. Avila et al., Phys. Lett. B **537**, 41 (2002)
31. N. Kwak et al., Phys. Lett. B **58**, 233 (1975)
32. U. Amaldi et al., Nucl. Phys. B **166**, 301 (1979)
33. E. Nagy et al., Nucl. Phys. B **150**, 221 (1979)
34. A. Breakstone et al., Phys. Rev. Lett. **54**, 2180 (1985)
35. M. Ambrosio et al., Phys. Lett. B **115**, 495 (1982)
36. A. Breakstone et al., Nucl. Phys. B **248**, 253 (1984)
37. C. Augier et al., Phys. Lett. B **316**, 448 (1993)
38. F. Abe et al., Phys. Rev. D **50**, 5518 (1993)
39. M. Bozzo et al., Phys. Lett. B **147**, 385 (1984)
40. M. Bozzo et al., Phys. Lett. B **155**, 197 (1985)
41. E710 Collaboration, N.M. Amos et al., Phys Lett. B **247**, 127 (1990)
42. C.D.F. Collaboration, F. Abe et al., Phys. Rev. D **50**, 5518 (1993)
43. DO Collaboration, V.M. Abazov et al., FERMILAB-PUB-12-263-E [arXiv:1206.0687 [hep-ex]]
44. R.E. Breedon et al., Phys. Lett. B **216**, 459 (1989)
45. D. Bernard et al., Phys. Lett. B **171**, 142 (1986)
46. Particle Data Group. http://pdg.lbl.gov
47. X. Zhan, Ph.D. thesis, Massachusetts Institute of Technology (2010) [arXiv:1108.4441[nucl-ex]]
48. X. Zhan et al., Phys. Lett. B **705**, 59 (2011)
49. Ch. Berger et al., Phys. Lett. B **35**, 85 (1971)

50. K.M. Hanson et al., Phys. Rev. D **8**, 753 (1973)
51. J. Arrington, W. Melnitchouk, J.A. Tron, Phys. Rev. C **76**, 035205 (2007)
52. A.S. Caroll et al., Phys. Lett. B **80**, 423 (1979)
53. Y. Akimov et al., Phys. Rev. D **12**, 3399 (1975)
54. G.G. Beznogikh et al., Phys. Lett. B **43**, 85 (1973)
55. D. Gross et al., Phys. Rev. Lett. **41**, 217 (1978)
56. A. Bujak et al., Phys. Rev. D **23**, 1895 (1981)
57. J.P. Burq et al., Nuc. Phys. B **187**, 205 (1981)
58. C.W. Akerlof et al., Phys. Rev. D **14**, 2864 (1976)
59. R. Rubinstein et al., Phys. Rev. D **30**, 1413 (1984)
60. R. Cool et al., Phys. Rev. D **24**, 2821 (1981)
61. A. Schiz et al., Phys. Rev. D **24**, 26 (1979)
62. M. Adamus et al., Phys. Lett. B **186**, 223 (1987)